

# Freezing-Enhanced Dissolution of Iron Oxides: Effects of Inorganic Acid Anions

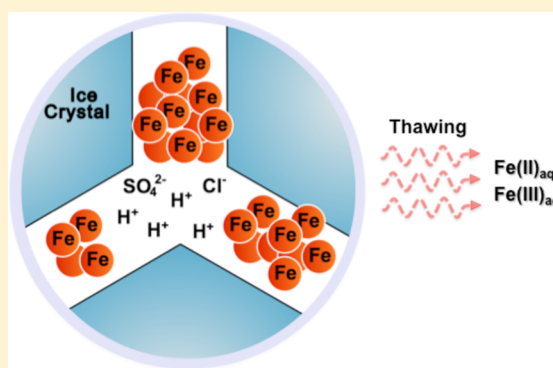
Daun Jeong,<sup>†</sup> Kitae Kim,<sup>‡</sup> Dae Wi Min,<sup>†</sup> and Wonyong Choi<sup>\*,†</sup>

<sup>†</sup>School of Environmental Science and Engineering, Pohang University of Science and Technology (POSTECH), Pohang 790-784, Korea

<sup>‡</sup>Korea Polar Research Institute, Incheon 406-840, Korea

**S** Supporting Information

**ABSTRACT:** Dissolution of iron from mineral dust particles greatly depends upon the type and amount of copresent inorganic anions. In this study, we investigated the roles of sulfate, chloride, nitrate, and perchlorate on the dissolution of maghemite and lepidocrocite in ice under both dark and UV irradiation and compared the results with those of their aqueous counterparts. After 96 h of reaction, the total dissolved iron in ice (pH 3 before freezing) was higher than that in the aqueous phase (pH 3) by 6–28 times and 10–20 times under dark and UV irradiation, respectively. Sulfuric acid was the most efficient in producing labile iron under dark condition, whereas hydrochloric acid induced the most dissolution of the total and ferrous iron in the presence of light. This ice-induced dissolution result was also confirmed with Arizona Test Dust (AZTD). In the freeze–thaw cycling test, the iron oxide samples containing chloride, nitrate, or perchlorate showed a similar extent of total dissolved iron after each cycling while the sulfate-containing sample rapidly lost its dissolution activity with repeating the cycle. This unique phenomenon observed in ice might be related to the freeze concentration of protons, iron oxides, and inorganic anions in the liquid-like ice grain boundary region. These results suggest that the ice-enhanced dissolution of iron oxides can be a potential source of bioavailable iron, and the acid anions critically influence this process.



## INTRODUCTION

Iron is an essential but limiting nutrient to marine organisms in about 30% of the open ocean (HNLC; high nutrient low chlorophyll).<sup>1–3</sup> Among 16 Tg of iron deposited to the open ocean each year, only a small portion of it (i.e., around 0.02 to 1 nM) is in a form bioavailable to marine organisms.<sup>4</sup> This lack of bioavailable iron is mainly caused by the low solubility of ferric iron, which is the most stable form at pH 8, and also by removal through adsorption on sinking particles.<sup>5,6</sup> The major source of iron in the open ocean is the atmospheric deposition of mineral dust aerosols, which accounts for 95% of the atmospheric iron budget.<sup>4,7</sup> Aeolian dust aerosols undergo various chemical and physical weathering processes that enhance their solubility and thus provide bioavailable iron upon deposition to the open ocean. Extensive laboratory, field, and model studies have been carried out to investigate the factors controlling iron dissolution processes and these include the effect of light, pH, organic and inorganic ligands, and the characteristics (e.g., source, size, structure, etc.) of iron-containing dust.<sup>7–10</sup>

Reactions in the ice matrix can undergo different pathways compared to the aqueous counterparts. Although an apparent frozen material seems completely solid, it may contain some amount of liquid when frozen above its “eutectic point”.<sup>11,12</sup> This liquid content exists between solid ice crystals and is often referred to as “liquid-like boundary” or “ice grain boundary”.

In this ice boundary region, solutes, protons, and dissolved gases can be extremely concentrated (i.e., freeze concentration effect), which provides a unique reaction environment that is very different from the normal aqueous media.<sup>13–15</sup> For example, nitrite oxidation has been reported to be accelerated by 10<sup>5</sup> times upon freezing.<sup>13</sup> It is interesting to note that even the exothermic hydration of 2-oxopropanoic acid to 2,2-dihydroxypropanoic proceeded down to 250 K in ice.<sup>16</sup> Our recent studies found that the dissolution of iron oxide particles can be greatly enhanced upon freezing both in the dark and under photoradiation because of the freeze concentration effect of protons, iron oxides, and organic ligands in the grain boundaries.<sup>17,18</sup> A similar ice-enhanced dissolution was also observed for manganese oxide.<sup>19</sup> The extent of iron (or manganese) release depended on the presence of light, pH, freezing temperature, surface area of iron oxides, and the type of organic ligands present.

Iron-containing atmospheric dust particles are one of the most efficient ice nuclei in forming cirrus clouds.<sup>20–22</sup> The presence of atmospheric dust facilitates the ice formation (i.e., heterogeneous freezing) at relatively low humidity and high temperature compared

Received: August 30, 2015

Revised: October 6, 2015

Accepted: October 7, 2015

Published: October 7, 2015

to a condition in which ice can form in the absence of any nuclei (i.e., homogeneous freezing).<sup>23,24</sup> Recent studies also indicate that ice residues frequently contain organic/inorganic compounds from anthropogenic or natural sources.<sup>25</sup> In the aqueous phase, these compounds can influence the dissolution of iron by forming mono- or multidentate complexes between the ligands and the iron oxide surface.<sup>6,8,26</sup> Therefore, iron oxides trapped in atmospheric ice might undergo unique chemical and physical reactions in the presence of these ligands.

In this study, we investigated the roles of inorganic acid anions on the dissolution of iron oxides in ice under both dark and UV irradiation. Atmospheric dust particles can often be coated with high concentrations of sulfate, chloride, and nitrate in the acidic deliquescence layer on the surface.<sup>27,28</sup> Moreover, many studies have reported the coexistence of these inorganic anions and dust particles in atmospheric ice residuals.<sup>21,22</sup> To better understand the roles of inorganic acid anions in producing bioavailable iron in ice, we conducted dissolution experiments with maghemite and lepidocrocite in both aqueous and ice phases in the presence of sulfate, chloride, nitrate, and perchlorate.

## MATERIALS AND METHODS

**Materials.** Maghemite (Aldrich, BET surface area 36 m<sup>2</sup>/g), lepidocrocite (LANXESS Corp, 75 m<sup>2</sup>/g), and Arizona fine test dust (Power Technology Inc., ISO 12103-1 A2 test dust) were used as received for iron oxide dissolution experiments. Arizona test dust (AZTD) is typically composed of 2–5 wt % of Fe<sub>2</sub>O<sub>3</sub> and has been used as a reference material for mineral dust. Detailed information on AZTD can be found at [www.powdertechologyinc.com](http://www.powdertechologyinc.com). Inorganic acids such as sulfuric acid, hydrochloric acid, nitric acid, and perchloric acid were all purchased from Aldrich and were diluted with ultrapure (18 MΩ cm) deionized water as desired.

**Experimental Procedures.** A total of 50 mL of 0.2 g/L iron oxide suspension was prepared in ultrapure (18 MΩcm) deionized water and sonicated for 3 min for better dispersion. After sonication, pH of the iron oxide suspensions was adjusted with H<sub>2</sub>SO<sub>4</sub>, HCl, HNO<sub>3</sub>, or HClO<sub>4</sub>. The initial pH condition was mainly adjusted to 3 in order to mimic a low pH atmospheric aerosol environment. Five mL of this suspension was placed in a quartz tube, sealed with septa, and put in a merry-go-round photolysis reactor in the ethanol bath set at −5 °C. The temperature of the ethanol bath was then gradually lowered to −20 °C (with a rate of 0.5 °C min<sup>−1</sup>) to prevent the breakage of the tubes. A 100-W mercury lamp (Ace Glass Inc.) surrounded by a pyrex jacket (transmitting λ > 300 nm) was immersed in an ethanol (transparent to the irradiation of λ > 300 nm) bath for uniform irradiation. The UV light intensity incident on the immersed quartz tube reactor was estimated to be 3.0 × 10<sup>−4</sup> Einstein min<sup>−1</sup> L<sup>−1</sup> (λ > 300 nm) by ferrioxalate actinometry.<sup>17</sup> For dissolution experiments under dark condition, 5 mL of the iron oxide suspension was placed in a conical tube (15 mL) and put in an ethanol bath cooled at −20 °C or kept at ambient temperature (20–25 °C) for aqueous samples. After each reaction time (i.e., 24, 48, 72, 96 h), sample tubes were thawed in warm water (40 °C) for further analysis. The thawing process was completed within 10 min and the thawed samples were filtered with a 0.45-μm filter to remove particles prior to the analysis of dissolved iron. The reprecipitation of dissolved iron was negligible within this time of the sample treatments. In the case of freeze–thaw cycling experiments, the experimental procedure was the same but the temperature of the ethanol bath was adjusted repeatedly between 25 °C and −20 °C every 12 h for 4 days. After each cycle, the sample tubes were withdrawn and analyzed.

**Analysis.** The dissolved iron was determined colorimetrically after filtering the suspension samples through a 0.45-μm filter. For ferrous (Fe<sup>2+</sup>) analysis, 2 mL of 1,10-phenanthroline and 1.5 mL of ammonium acetate buffer were added to a 5-mL conical tube containing 1.5 mL of the sample. The same samples were also analyzed for the total dissolved iron (Fe<sub>tot</sub> = Fe<sup>2+</sup> + Fe<sup>3+</sup>) by adding 100 μL of hydroxylamine hydrochloride for ferric reduction to ferrous. After an hour, absorbance of the samples was measured with a UV/visible spectrophotometer (Libra S22, Biochrom) at 510 nm. ζ-Potential and hydrodynamic diameter of the iron oxide samples were measured using an electrophoretic light-scattering spectrophotometer (ELS 8000, Otsuka). The extent of aggregation of iron oxides was analyzed with TEM. The TEM samples were prepared using a freeze-drying method to minimize a possible effect of drying process on the aggregation state of the iron oxide particles. One drop of iron oxide suspension containing the acid anions (i.e., Cl<sup>−</sup> or SO<sub>4</sub><sup>2−</sup>) was applied to a TEM sample grid, frozen at −80 °C, and then dried in a freeze drier for 12 h prior to TEM analysis.

## RESULTS AND DISCUSSION

**Anion Effects on Iron Oxide Dissolution in Ice under Dark Condition.** Figure 1 compares the production of total

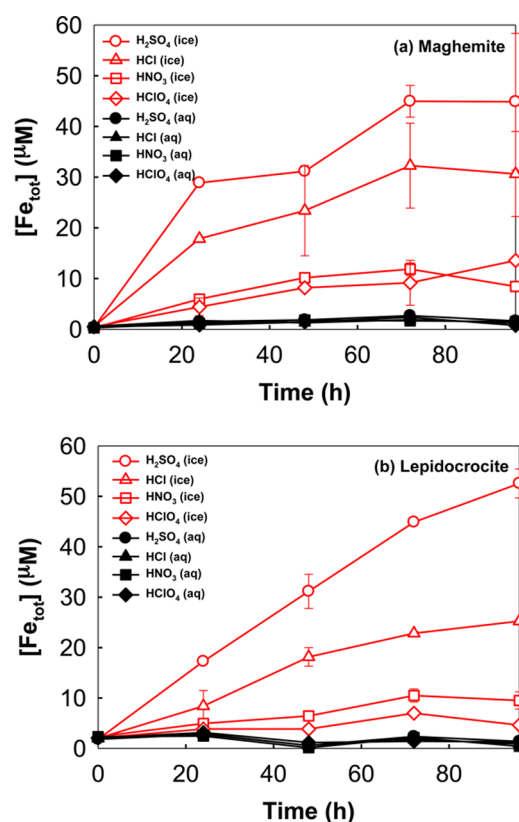


**Figure 1.** Production of total dissolved iron from (a) maghemite ( $\gamma$ -Fe<sub>2</sub>O<sub>3</sub>) and (b) lepidocrocite ( $\gamma$ -FeOOH) under dark condition in the presence of various inorganic anions after reaction in water (25 °C) and ice (−20 °C). Experimental conditions: pH<sub>i</sub> = 3 (±0.05), [iron oxide] = 0.2 g/L.

dissolved iron from the dissolution of maghemite (a) and lepidocrocite (b) in the presence of various acid anions both in the ice and aqueous phases. The dissolved iron concentration was markedly enhanced in the ice phase for all types of acids used, while a negligible concentration of dissolved iron was

observed in the aqueous phase. In the absence of light (Figure 1), most of the dissolved iron was in the ferric form, which indicates a nonreductive dissolution.<sup>18</sup> The iron dissolving efficiency of the inorganic anions was in the order of sulfate > chloride > nitrate  $\approx$  perchlorate. After 96 h of reaction of maghemite in ice, the samples with sulfate and chloride yielded the highest concentrations ( $45(\pm 13)$   $\mu\text{M}$  and  $31(\pm 8)$   $\mu\text{M}$ , respectively) of total dissolved iron, while nitrate and perchlorate produced much lesser amounts ( $8.4(\pm 1)$   $\mu\text{M}$  and  $13$   $\mu\text{M}$ , respectively). In the aqueous phase, approximately  $1$   $\mu\text{M}$  of labile iron was released with all types of inorganic anions. This ice-induced iron dissolution was also observed for lepidocrocite (Figure 1b) and AZTD (Figure 2). The extent of iron dissolution in ice was

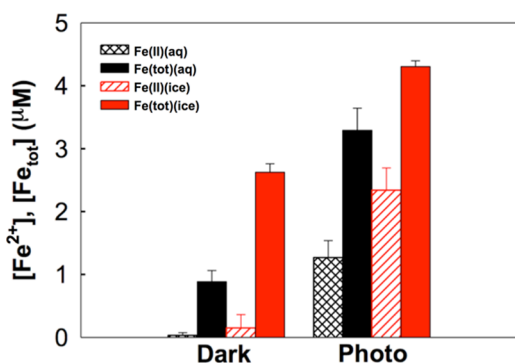
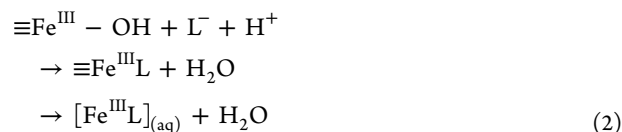
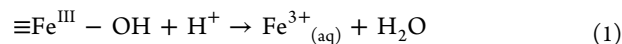


**Figure 2.** Comparison of total dissolved iron and ferrous ion from AZTD (Arizona test dust) between water ( $25$   $^{\circ}\text{C}$ ) and ice ( $-20$   $^{\circ}\text{C}$ ) under dark and UV irradiation. Experimental conditions:  $\text{pH}_i = 3 \pm 0.05$  (adjusted with  $\text{H}_2\text{SO}_4$ ),  $[\text{AZTD}] = 2$   $\text{g/L}$ , reaction time 48 h.

dependent upon the initial acid anion concentration in the sample. With increasing the concentration of sulfate and chloride (i.e., up to  $10$   $\text{mM}$ ), the dissolved iron increased (Supporting Information (SI) Figure S1). Another factor that might influence the dissolution rate is the surface area of iron oxide samples. Although a higher dissolution rate is expected with a higher surface area, lepidocrocite (of which BET surface area is twice as large as that of maghemite) exhibited a lower dissolution rate than maghemite (compare Figure 1a vs 1b). This implies that other factors such as the crystallinity and inorganic acid anion are more critical in determining the dissolution rate.

The accelerated dissolution of iron oxides in ice under dark condition can be related to the “freeze concentration effect” of iron oxides, protons, and inorganic anions in the liquid-like ice grain boundary region. Studies showed that dissolved ions are distributed unequally between the ice and aqueous phases when freezing. This inequality develops an electric potential (so-called “freezing potential”), which induces  $\text{OH}^-$  or  $\text{H}_3\text{O}^+$  to be preferentially accumulated in the ice grain boundary region resulting in a pH change.<sup>29</sup> For example,  $\text{NaCl}$  induces the accumulation of  $\text{OH}^-$  ions (pH increase) in the liquid-like boundary region through the preferential incorporation of  $\text{Cl}^-$  ions in the ice matrix (i.e., negative potential in the ice side and positive potential in the liquid side) while  $\text{Na}_2\text{SO}_4$  may have the opposite effect (inducing pH decrease).<sup>30,31</sup> However, in our study, the presence of iron oxides makes the chemistry more complex since the iron oxides, which contain amphoteric surface hydroxyl groups, can buffer the change of pH to some extent. It seems that the freezing-induced accumulation of protons<sup>32,33</sup> and anions can enhance the interfacial iron dissolution processes (eqs 1 and 2) in the ice grain boundary region. The increased

proton mobility in frozen media could be an important factor in the dissolution process. Proton mobility in a frozen media has been reported to be comparable to or even greater than that in the liquid counterpart.<sup>34</sup> As expected, the initial pH had significant influence on enhancing the total dissolved iron in ice, and the iron dissolution was higher at lower pH (SI Figure S2), which should be ascribed to the proton-assisted dissolution (eq 1).



Because the pH of all other dissolution experiments was controlled at pH 3 in this study (Figure 1), the observed difference in the iron dissolution rate with different acid anions should be ascribed mainly to the effect of the anions, ligand-promoted dissolution (eq 2). The presence of anion ligands may modify the dissolution process of iron oxides depending on their strength and mode of adsorption on the solid oxide surfaces.

The nonreductive ligand-promoted dissolution of iron oxides is initiated by the adsorption of inorganic ligand on the iron oxide surface. This weakens the Fe–O bonds and the ferric complex is detached from the iron oxide surface to be dissolved into the bulk solution (eq 2). Many studies have reported metal oxide dissolution promoted by sulfate and chloride. In particular, sulfate can strongly adsorb on oxide surfaces by displacing the surface hydroxyl groups and forming monodentate or bidentate complexes<sup>6,35,36</sup> with surface iron.<sup>37</sup> Being a divalent ion, sulfate tends to show stronger affinity on iron oxide surfaces and also promote more proton adsorption compared to monovalent anions.<sup>37,38</sup> Therefore, sulfate can extract labile iron from iron oxides more efficiently compared to monovalent ions.<sup>32,38</sup> The ice-enhanced release of labile iron in the presence of sulfate was also confirmed with AZTD, which is a reference material for mineral dust (Figure 2). Different types of monovalent ions also show disparate affinities on iron oxide surfaces. Among the monovalent ions, studies showed that chloride accelerates the dissolution of iron by forming strong complexation with ferric species and by directly coordinating to the solid oxide surface. In contrast, perchlorate and nitrate adsorb on the surface by forming weak outer-sphere complexes and are therefore considered inert electrolytes compared to sulfate and chloride.<sup>6,26,37,38</sup> In the ice grain boundary regions, sulfate, chloride, and protons can be concentrated, leading to both ligand- and proton-assisted dissolution of iron. Moreover, the enhanced protonation of the iron oxide surface in the grain boundary increases the positive surface charge density, which further facilitates the electrostatic attraction of negatively charged chloride and sulfate anions.<sup>6,26</sup>

**Anion Effects on Iron Oxide Dissolution in Ice under UV Light.** Iron oxide dissolution experiments were also performed in the presence of light to investigate the solar irradiation effect, and the results are shown in Figure 3. In the ice phase, the production of both total dissolved iron and ferrous ion was markedly enhanced in the presence of light compared to the dark dissolution, which implies that a photoreductive dissolution mechanism is operating in this case.<sup>17</sup> This trend was also confirmed with the dissolution from AZTD in the presence of sulfate (Figure 2). It should be noted that, under irradiation, the order of iron dissolution efficiency of the inorganic acid anions

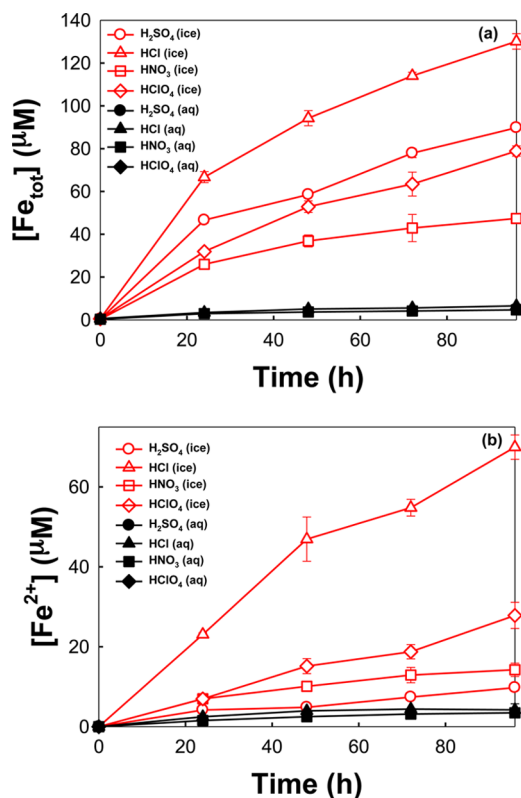
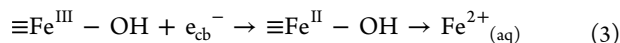


**Figure 3.** Photoirradiation-induced production of (a) total dissolved iron and (b) ferrous (Fe(II)) ion from maghemite under UV irradiation in the presence of various inorganic anions after reaction in water (25 °C) and ice (-20 °C). Experimental conditions:  $pH_i = 3 (\pm 0.05)$ ,  $[\gamma-Fe_2O_3] = 0.2$  g/L.

decreases in the order of chloride > sulfate > perchlorate > nitrate, which is different from that in the dark condition.

The photoreductive dissolution of iron oxide in ice can be largely explained by two mechanisms: the photoexcitation of surface iron complexes (e.g., ligand-to-metal charge transfer<sup>39–41</sup>) and the bandgap excitation of semiconducting iron oxides.<sup>17</sup> As for the first case, the surface complexation of ligands promotes the photodissolution of iron.<sup>39–41</sup> In the absence of ligands, surface coordinated water or hydroxyl groups donate an electron to surface ferric ion producing surface-bound ferrous species,<sup>42</sup> which should be subsequently detached from the surface. The concentration of inorganic anions such as sulfate and chloride in the ice grain boundary region should promote their surface complexation, which subsequently accelerates the iron dissolution. On the other hand, the semiconductor model is based on the bandgap excitation of iron oxide with generating electron–hole pairs in the oxide lattice. The photogenerated conduction band (CB) electrons reduce the surface ferric ions (eq 3), while the holes can be scavenged by electron donors present in the surface region.



Among inorganic acid anions, chloride may react with the photogenerated valence band (VB) holes ( $Cl^- + h_{vb}^+ \rightarrow Cl^\bullet$ :  $E^0(Cl^\bullet/Cl^-) = 2.2 V_{NHE}$ ) to enhance the overall photoreductive dissolution of iron oxide, which may explain why the photodissolution of maghemite was the most efficient in the presence of chloride (see Figure 3). The VB edge potential of maghemite is positive enough to oxidize chloride ion to chlorine radical ( $E_{vb}(\text{maghemite}) = 2.6 V_{NHE}$ ).<sup>43</sup> This explanation is supported

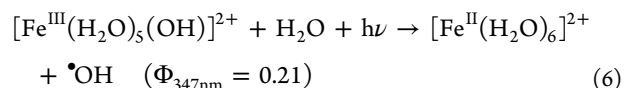
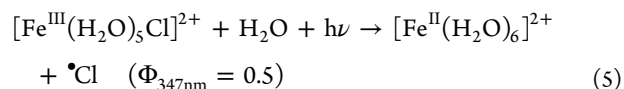
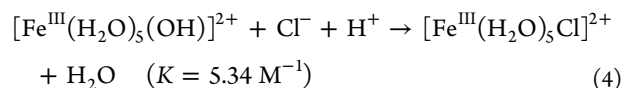
**Table 1.** Photo-Dissolution of Iron (Fe(II) + Fe(III)) from Maghemite in Ice in the Presence of Various Inorganic Anions<sup>a</sup>

anion type	dissolved iron ( $\mu M$ )		
	Fe(II)	Fe(III)	total Fe
$SO_4^{2-}$	$9.8 \pm 0.7$ (11%) <sup>b</sup>	$80.0 \pm 0.4$	$89.8 \pm 1.1$
$Cl^-$	$70.0 \pm 3.0$ (54%)	$60.2 \pm 0.6$	$130.1 \pm 3.6$
$NO_3^-$	$14.2 \pm 1.7$ (30%)	$33.2 \pm 0.8$	$47.4 \pm 0.9$
$ClO_4^-$	$27.8 \pm 3.3$ (35%)	$51.0 \pm 5.7$	$78.9 \pm 2.4$

<sup>a</sup>Experimental conditions:  $[\gamma-Fe_2O_3] = 0.2$  g/L, pH 3, reaction time 96 h under UV irradiation at -20 °C. <sup>b</sup>Percentage of Fe(II) in the total dissolved iron.

by the data shown in Table 1. Although the photoproduction of total dissolved iron in ice was highest with chloride, the production of Fe(III) was highest with sulfate (as in the dark dissolution in Figure 1). Note that the photogeneration of Fe(II) is outstanding with chloride compared with other anions, which supports the role of chloride as a hole scavenger. The highest efficiency of maghemite/chloride system for the photodissolution can be explained by the semiconductor mechanism where chlorides serve as a hole scavenger. Although this semiconductor mechanism has been suggested as not effective because of the fast charge recombination in iron oxide,<sup>44,45</sup> the ice system where the hole scavengers (e.g., chloride) can be highly concentrated in the ice grain boundary may be different from the aqueous system. Moreover, the iron oxide particles are excluded from the ice crystals and extensively aggregated in the grain boundary region.<sup>17</sup> This agglomeration of semiconductor nanoparticles (iron oxide) may facilitate the charge-pair separation by electron hopping through the particle grain boundaries when they are trapped in the frozen phase.<sup>17,46</sup>

An alternative explanation for the higher photogeneration of Fe(II) in the presence of chloride is the photoactivity of Fe(III)–Cl complex that leads to the generation of ferrous ions. Once ferric ions ( $[Fe^{III}(H_2O)_5(OH)]^{2+}$  or simply  $FeOH^{2+}$ ) are dissolved through eqs 1 and 2, they can be complexed with chloride ions (eq 4). These Fe(III)–Cl complexes ( $[Fe^{III}(H_2O)_5Cl]^{2+}$  or simply  $FeCl^{2+}$ ) are photoactive at UV and visible regions to reduce ferric to ferrous ion.<sup>7,47</sup> At the low pH condition, the dominant species in the presence of chloride are  $FeCl^{2+}$  and  $FeCl_2^+$  with  $FeOH^{2+}$  being present only in very low level.  $FeCl^{2+}$  can be photoreduced under solar irradiation (eq 5), which is twice as active as the photoreduction of  $FeOH^{2+}$  (eq 6). Such complex formation of  $FeCl^{2+}$  should be more favored in the ice grain boundary region (where ferric ions and chlorides are concentrated) with facilitating the photogeneration of  $Fe^{2+}$  ions. Both the iron complex model and the semiconductor excitation model can explain the higher photoproduction of Fe(II) in the presence of chloride.



where values of  $K$  and  $\Phi$  are from ref 48.

On the other hand, in the presence of nitrate that is a very weak complexing ligand, the reductive process can be suppressed by a strong oxidant (i.e.,  $\bullet\text{OH}$ ) produced by the photolysis of nitrate.<sup>50,49</sup> Similarly, Fe(III)–sulfate complexes may also have photochemical properties suppressing the reduction of ferric to ferrous ions.<sup>7</sup> The adsorption of sulfate on iron oxide surfaces replaces OH groups,<sup>37</sup> which are known to reduce ferric ions.<sup>42</sup> Accordingly, sulfate that showed the highest iron dissolution in the dark also produced the highest amount of Fe(III) under the photoirradiation but the lowest amount of Fe(II) (see Table 1). This indicates that the Fe(III)–sulfate complexes retard the photo-reduction of ferric species as was also observed in case of the photodissolution of  $\alpha\text{-FeOOH}$ .<sup>7</sup>

**Simulated Freeze–Thaw Cycling Process.** Iron oxide particles may undergo a series of freeze–thaw cycles in the natural environment. To simulate the freezing-induced weathering process, the iron oxide suspensions were frozen and then thawed for repeated cycles and were analyzed for total dissolved iron after each process (Figure 4). After the first 12 h of reaction

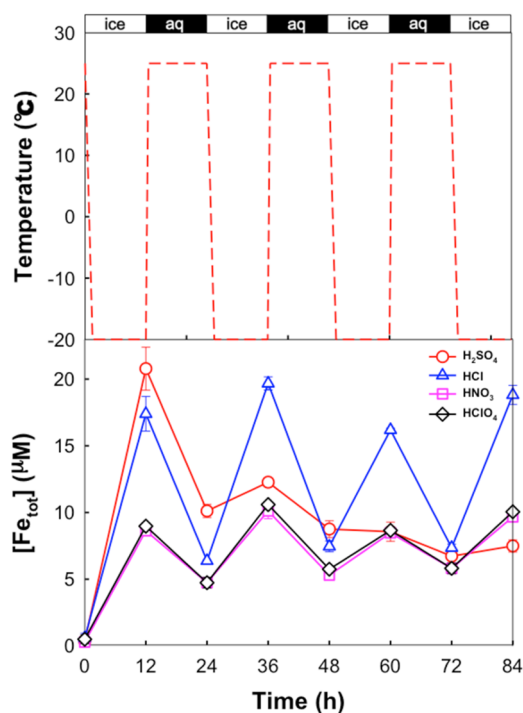


**Figure 4.** (a) Temperature variation profile and (b) the accompanying production of total dissolved iron from maghemite ( $\gamma\text{-Fe}_2\text{O}_3$ ) during the freeze–thaw cycling experiment under the dark condition. Aqueous phase maintained at 25 °C and ice phase at –20 °C. Experimental conditions:  $\text{pH}_i = 3 \pm 0.05$ ,  $[\gamma\text{-Fe}_2\text{O}_3] = 0.2 \text{ g/L}$ .

in ice, a significant amount of dissolved iron was observed for all types of acid anions, as expected. For the next 12 h, the samples were maintained in an aqueous phase by raising the temperature from –20 to 25 °C. After 12 h in a thawed state, approximately half of total dissolved iron was reduced from its initial value for all types of anion samples. This should be ascribed to the precipitation of ferric ions which have a low solubility at pH 3.<sup>51</sup> During the four successive freeze–thaw cycles, the iron dissolution and precipitation showed a reversible behavior (i.e., dissolution upon freezing and reprecipitation after thawing) in the presence of chloride, nitrate, or perchlorate. It seems that the number of the freeze–thaw cycles has an insignificant influence on the steady-

state level of dissolved iron with these acid anions. However, the sulfate system showed a markedly different behavior. In the presence of sulfate, the behavior of iron dissolution and precipitation was irreversible and the freezing-induced dissolution of iron was significantly reduced after the first freeze–thaw cycle and gradually decreased with repeating the cycle. As a result, the iron dissolution with sulfate was the lowest after the fourth cycle among the compared samples while the presence of sulfate induced the highest level of dissolved iron after the first cycle.

This unique iron dissolution profile obtained in the presence of sulfate might be ascribed to the difference in the extent of aggregation of maghemite particles. Table 2 shows the  $\zeta$ -potential

**Table 2. Properties of Maghemite before and after Reaction in Water and Ice<sup>a</sup>**

anion type	$\zeta$ -potential (mV)		hydrodynamic diameter (nm)	
	initial		initial	ice <sup>b</sup>
$\text{SO}_4^{2-}$	$14 \pm 0$		$1303 \pm 137$	$1934 \pm 10$
$\text{Cl}^-$	$44 \pm 1$		$512 \pm 18$	$672 \pm 30$
$\text{NO}_3^-$	$43 \pm 2$		$451 \pm 29$	$497 \pm 61$
$\text{ClO}_4^-$	$52 \pm 4$		$503 \pm 112$	$420 \pm 26$

<sup>a</sup>Experimental conditions:  $[\gamma\text{-Fe}_2\text{O}_3] = 0.2 \text{ g/L}$ , pH 3, reaction time 6 h under dark condition at 25 °C and –20 °C. <sup>b</sup>Hydrodynamic diameter measured after 6 h of reaction.

and the dynamic light scattering (DLS) measurements of maghemite at the initial stage and after 6 h reaction in ice and aqueous phase, respectively. In the presence of sulfate, the initial  $\zeta$ -potential of maghemite was the lowest (14 mV) among 4 types of inorganic acid anions and the hydrodynamic diameter was the largest both before and after the reaction in the aqueous and ice phase. In particular, the size of sulfate-containing iron oxide agglomerates after reaction in ice was about 5 times larger than those of chloride-, nitrate-, or perchlorate-containing iron oxide sample. This extensive aggregation of iron oxide particles caused by sulfate was also confirmed by TEM images (see Figure 5).

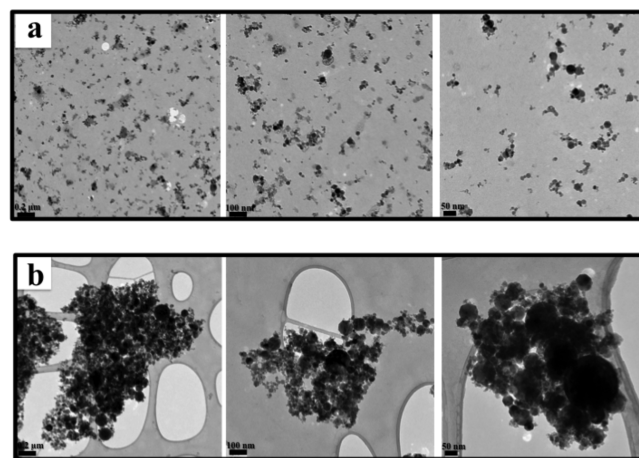


**Figure 5.** TEM images of maghemite particles in the presence of (a) chloride and (b) sulfate after 6 h reaction in the ice phase (–20 °C) under dark condition. Experimental conditions:  $\text{pH}_i = 3 \pm 0.05$ ,  $[\gamma\text{-Fe}_2\text{O}_3] = 0.2 \text{ g/L}$ .

On the other hand, the iron oxide samples containing other acid anions showed much less change in the hydrodynamic size and

the agglomeration after the freeze–thaw cycle. Being a divalent anion, sulfate has a high affinity for positively charged iron oxide surface and subsequently reduces the positive surface charge more efficiently than other monovalent anion.<sup>37,38</sup> This is reflected in the lowest zeta-potential of maghemite in the presence of sulfate (see Table 2). In addition, the freeze concentration of divalent sulfate ions within the ice grain boundary region highly enhances the ionic strength, which induces the aggregation of iron oxide particles more efficiently than monovalent ions. As a result, the electrostatic repulsion force between iron oxide particles is weakest in the presence of sulfate and therefore the largest agglomerates are formed.<sup>35,37</sup> The iron oxide particles are forced to be aggregated in the confined space of ice grain boundaries but might be deaggregated after thawing. However, the presence of sulfate seems to stabilize the state of agglomeration as shown in Figure 5b. The large aggregates reduce the number of active surface sites eventually diminishing the dissolution rate.<sup>52,53</sup>

**Environmental Implications.** The present study demonstrates that the presence and kind of inorganic acid anions can critically influence the freezing-induced dissolution of bioavailable iron from mineral particles both in the dark and under photoirradiation. The ice-enhanced dissolution of iron oxides in the dark condition was most efficient in the presence of sulfate, whereas the dissolution under the photoirradiation was the highest in the presence of chloride. During the freeze–thaw cycle, the presence of sulfate facilitated the aggregation of iron oxide particles with gradually reducing the iron dissolution efficiency. Iron-containing dust particles in the atmosphere can be transported long-range and undergo multiple freeze–thaw cycles.<sup>14,54</sup> In the presence of acid anions, the pH of iron-containing aerosols may decrease to pH 1–2.<sup>54</sup> Thus, acidic aerosols containing inorganic anions have been suggested as a source of bioavailable iron.<sup>7,8</sup> This study showed that the extent of iron dissolution is markedly enhanced in the ice phase in the presence of sulfate or chloride. Therefore, any changes in the anthropogenic and natural emissions of sulfur- and chlorine-containing compounds, which are the precursors of inorganic anions in the atmosphere, might be related with modifying the freezing-induced dissolution of iron-containing atmospheric aerosols. The freezing-induced dissolution of iron oxides is suggested as an important source of bioavailable iron that will eventually influence the ocean carbon cycle upon deposition to the open ocean.<sup>1,4</sup> Further laboratory studies and field observations should be carried out to investigate and assess the effects of various inorganic and organic ligands on the freezing-induced dissolution of iron oxides in cold environments such as the upper atmosphere and polar regions.

## ■ ASSOCIATED CONTENT

### ● Supporting Information

The Supporting Information is available free of charge on the ACS Publications website at DOI: 10.1021/acs.est.5b04211.

Effects of acid anion concentrations and pH on the total dissolved iron production from maghemite under dark (PDF).

## ■ AUTHOR INFORMATION

### Corresponding Author

\*E-mail: wchoi@postech.edu; tel.: +82-54-279-2283; fax: +82-54-279-8299.

### Notes

The authors declare no competing financial interest.

## ■ ACKNOWLEDGMENTS

Funding for this work was provided by the Global Research Laboratory program (2014K1A1A2041044) supported by the Korea government (MSIP) through NRF, Korea Polar Research Institute (KOPRI) project (PP15010), and the KOPRI “Polar Academic Program (PAP)”.

## ■ REFERENCES

- (1) Martin, J. H.; Gordon, R. M.; Fitzwater, S. E. Iron in Antarctic waters. *Nature* **1990**, *345*, 156–158.
- (2) Boyd, P. W.; Jickells, T.; Law, C. S.; Blain, S.; Boyle, E. A.; Buesseler, K. O.; Coale, K. H.; Cullen, J. J.; De Baar, H. J. W.; Follows, M.; Harvey, M.; Lancelot, C.; Levasseur, M.; Owens, N. P. J.; Pollard, R.; Rivkin, R. B.; Sarmiento, J.; Schoemann, V.; Smetacek, V.; Takeda, S.; Tsuda, A.; Turner, S.; Watson, A. J. Mesoscale iron enrichment experiments 1993–2005: Synthesis and future directions. *Science* **2007**, *315*, 612–617.
- (3) Shi, Z.; Krom, M. D.; Jickells, T. D.; Bonneville, S.; Carlsaw, K. S.; Mihalopoulos, N.; Baker, A. R.; Benning, L. G. Impacts on iron solubility in the mineral dust by processes in the source region and the atmosphere: A review. *Aeolian Research* **2012**, *5*, 21–42.
- (4) Turner, D. R.; Hunter, K. A. *The Biogeochemistry of Iron in Seawater*; John Wiley & Sons: Chichester, UK, 2001; Vol. 7, p 396.
- (5) Johnson, K. S.; Gordon, R. M.; Coale, K. H. What controls dissolved iron concentrations in the world ocean? *Mar. Chem.* **1997**, *57*, 137–161.
- (6) Cornell, R. M.; Schwertmann, U. *The Iron Oxides: Structure, Properties, Reactions, Occurrence and Uses*; Wiley-VCH: New York, 1996.
- (7) Rubasinghege, G.; Lentz, R. W.; Scherer, M. M.; Grassian, V. H. Simulated atmospheric processing of iron oxyhydroxide minerals at low pH: Roles of particle size and acid anion in iron dissolution. *Proc. Natl. Acad. Sci. U. S. A.* **2010**, *107*, 6628–6633.
- (8) Chen, H.; Grassian, V. H. Iron dissolution of dust source materials during simulated acidic processing: The effect of sulfuric, acetic, and oxalic acids. *Environ. Sci. Technol.* **2013**, *47*, 10312–10321.
- (9) Cwiertny, D. M.; Young, M. A.; Grassian, V. H. Chemistry and photochemistry of mineral dust aerosol. *Annu. Rev. Phys. Chem.* **2008**, *59*, 27–51.
- (10) Shi, Z.; Bonneville, S.; Krom, M. D.; Carlsaw, K. S.; Jickells, T. D.; Baker, A. R.; Benning, L. G. Iron dissolution kinetics of mineral dust at low pH during simulated atmospheric processing. *Atmos. Chem. Phys.* **2011**, *11*, 995–1007.
- (11) Pincock, R. E.; Kiovsky, T. E. Kinetics of reactions in frozen solutions. *J. Chem. Educ.* **1966**, *43*, 358–360.
- (12) Takenaka, N.; Bandow, H. Chemical kinetics of reactions in the unfrozen solution of ice. *J. Phys. Chem. A* **2007**, *111*, 8780–8786.
- (13) Takenaka, N.; Ueda, A.; Maeda, Y. Acceleration of the rate of nitrite oxidation by freezing in aqueous solution. *Nature* **1992**, *358*, 736–738.
- (14) Grannas, A. M.; Jones, A. E.; Dibb, J.; Ammann, M.; Anastasio, C.; Beine, H. J.; Bergin, M.; Bottenheim, J.; Boxe, C. S.; Carver, G.; Chen, G.; Crawford, J. H.; Dominé, F.; Frey, M. M.; Guzmán, M. I.; Heard, D. E.; Helmig, D.; Hoffmann, M. R.; Honrath, R. E.; Huey, L. G.; Hutterli, M.; Jacobi, H. W.; Klán, P.; Lefer, B.; McConnell, J.; Plane, J.; Sander, R.; Savarino, J.; Shepson, P. B.; Simpson, W. R.; Sodeau, J. R.; Von Glasow, R.; Weller, R.; Wolff, E. W.; Zhu, T. An overview of snow photochemistry: Evidence, mechanisms and impacts. *Atmos. Chem. Phys.* **2007**, *7*, 4329–4373.
- (15) Kim, K.; Choi, W. Enhanced Redox Conversion of Chromate and Arsenite in Ice. *Environ. Sci. Technol.* **2011**, *45*, 2202–2208.
- (16) Guzman, M. I.; Hildebrandt, L.; Colussi, A. J.; Hoffmann, M. R. Cooperative hydration of pyruvic acid in ice. *J. Am. Chem. Soc.* **2006**, *128*, 10621–10624.
- (17) Kim, K.; Choi, W.; Hoffmann, M. R.; Yoon, H. I.; Park, B. K. Photoreductive Dissolution of Iron Oxides Trapped in Ice and Its Environmental Implications. *Environ. Sci. Technol.* **2010**, *44*, 4142–4148.

- (18) Jeong, D.; Kim, K.; Choi, W. Accelerated dissolution of iron oxides in ice. *Atmos. Chem. Phys.* **2012**, *12*, 11125–11133.
- (19) Kim, K.; Yoon, H. I.; Choi, W. Enhanced Dissolution of Manganese Oxide in Ice Compared to Aqueous Phase under Illuminated and Dark Conditions. *Environ. Sci. Technol.* **2012**, *46*, 13160–13166.
- (20) Cziczo, D. J.; Froyd, K. D. Sampling the composition of cirrus ice residuals. *Atmos. Res.* **2014**, *142*, 15–31.
- (21) Cziczo, D. J.; Froyd, K. D.; Hoose, C.; Jensen, E. J.; Diao, M. H.; Zondlo, M. A.; Smith, J. B.; Twohy, C. H.; Murphy, D. M. Clarifying the Dominant Sources and Mechanisms of Cirrus Cloud Formation. *Science* **2013**, *340*, 1320–1324.
- (22) DeMott, P. J.; Cziczo, D. J.; Prenni, A. J.; Murphy, D. M.; Kreidenweis, S. M.; Thomson, D. S.; Borys, R.; Rogers, D. C. Measurements of the concentration and composition of nuclei for cirrus formation. *Proc. Natl. Acad. Sci. U. S. A.* **2003**, *100*, 14655–14660.
- (23) Archuleta, C. M.; DeMott, P. J.; Kreidenweis, S. M. Ice nucleation by surrogates for atmospheric mineral dust and mineral dust/sulfate particles at cirrus temperatures. *Atmos. Chem. Phys.* **2005**, *5*, 2617–2634.
- (24) DeMott, P. J.; Rogers, D. C.; Kreidenweis, S. M. The susceptibility of ice formation in upper tropospheric clouds to insoluble aerosol components. *J. Geophys. Res.* **1997**, *102*, 19575–19584.
- (25) Kamphus, M.; Ettner-Mahl, M.; Klimach, T.; Drewnick, F.; Keller, L.; Cziczo, D. J.; Mertes, S.; Borrmann, S.; Curtius, J. Chemical composition of ambient aerosol, ice residues and cloud droplet residues in mixed-phase clouds: single particle analysis during the Cloud and Aerosol Characterization Experiment (CLACE 6). *Atmos. Chem. Phys.* **2010**, *10*, 8077–8095.
- (26) Cornell, R. M.; Posner, A. M.; Quirk, J. P. Kinetics and mechanisms of the acid dissolution of goethite ( $\alpha$ -FeOOH). *J. Inorg. Nucl. Chem.* **1976**, *38*, 563–567.
- (27) Sullivan, R. C.; Guazzotti, S. A.; Sodeman, D. A.; Tang, Y.; Carmichael, G. R.; Prather, K. A. Mineral dust is a sink for chlorine in the marine boundary layer. *Atmos. Environ.* **2007**, *41*, 7166–7179.
- (28) Sullivan, R. C.; Guazzotti, S. A.; Sodeman, D. A.; Prather, K. A. Direct observations of the atmospheric processing of Asian mineral dust. *Atmos. Chem. Phys.* **2007**, *7*, 1213–1236.
- (29) Workman, E. J.; Reynolds, S. E. Electrical Phenomena Occurring during the Freezing of Dilute Aqueous Solutions and Their Possible Relationship to Thunderstorm Electricity. *Phys. Rev.* **1950**, *78*, 254–259.
- (30) Cobb, A. W.; Gross, G. W. Interfacial Electrical Effects Observed during Freezing of Dilute Electrolytes in Water. *J. Electrochem. Soc.* **1969**, *116*, 796–804.
- (31) Robinson, C.; Boxe, C. S.; Guzman, M. I.; Colussi, A. J.; Hoffmann, M. R. Acidity of frozen electrolyte solutions. *J. Phys. Chem. B* **2006**, *110*, 7613–7616.
- (32) Teir, S.; Revitzer, H.; Eloneva, S.; Fogelholm, C. J.; Zevenhoven, R. Dissolution of natural serpentinite in mineral and organic acids. *Int. J. Miner. Process.* **2007**, *83*, 36–46.
- (33) Hamer, M.; Graham, R. C.; Amrhein, C.; Bozhilov, K. N. Dissolution of ripidolite (Mg, Fe-chlorite) in organic and inorganic acid solutions. *Soil Sci. Soc. Am. J.* **2003**, *67*, 654–661.
- (34) Takenaka, N.; Ueda, A.; Daimon, T.; Bandow, H.; Dohmaru, T.; Maeda, Y. Acceleration mechanism of chemical reaction by freezing: The reaction of nitrous acid with dissolved oxygen. *J. Phys. Chem.* **1996**, *100*, 13874–13884.
- (35) Rao, S. M.; Sridharan, A. Mechanism of sulfate adsorption by kaolinite. *Clays Clay Miner.* **1984**, *32*, 414–418.
- (36) Zhu, M. Q.; Northrup, P.; Shi, C. Y.; Billinge, S. J. L.; Sparks, D. L.; Waychunas, G. A. Structure of Sulfate Adsorption Complexes on Ferrihydrite. *Environ. Sci. Technol. Lett.* **2014**, *1*, 97–101.
- (37) Harrison, J. B.; Berkheiser, V. E. Anion interactions with freshly prepared hydrous iron oxides. *Clays Clay Miner.* **1982**, *30*, 97–102.
- (38) Rietra, R. P. J. J.; Hiemstra, T.; van Riemsdijk, W. H. Electrolyte anion affinity and its effect on oxyanion adsorption on goethite. *J. Colloid Interface Sci.* **2000**, *229*, 199–206.
- (39) Waite, T. D.; Morel, F. M. M. Photoreductive Dissolution of Colloidal Iron Oxides in Natural Waters. *Environ. Sci. Technol.* **1984**, *18*, 860–868.
- (40) Voelker, B. M.; Morel, F. M. M.; Sulzberger, B. Iron redox cycling in surface waters: Effects of humic substances and light. *Environ. Sci. Technol.* **1997**, *31*, 1004–1011.
- (41) Borer, P.; Sulzberger, B.; Hug, S. J.; Kraemer, S. M.; Kretzschmar, R. Photoreductive Dissolution of Iron(III) (Hydr)oxides in the Absence and Presence of Organic ligands: Experimental Studies and Kinetic Modeling. *Environ. Sci. Technol.* **2009**, *43*, 1864–1870.
- (42) Miller, W. L.; King, D. W.; Lin, J.; Kester, D. R. Photochemical redox cycling of iron in coastal seawater. *Mar. Chem.* **1995**, *50*, 63–77.
- (43) Beydoun, D.; Amal, R.; Low, G.; Mcevoy, S. Occurrence and prevention of photodissolution at the phase junction of magnetite and titanium dioxide. *J. Mol. Catal. A: Chem.* **2002**, *180*, 193–200.
- (44) Leland, J. K.; Bard, A. J. Photochemistry of colloidal semiconducting iron oxide polymorphs. *J. Phys. Chem.* **1987**, *91*, 5076–5083.
- (45) Cherepy, N. J.; Liston, D. B.; Lovejoy, J. A.; Deng, H.; Zhang, J. Z. Ultrafast studies of photoexcited electron dynamics in  $\gamma$ - and  $\alpha$ -Fe<sub>2</sub>O<sub>3</sub> semiconductor nanoparticles. *J. Phys. Chem. B* **1998**, *102*, 770–776.
- (46) Lakshminarasimhan, N.; Kim, W.; Choi, W. Effect of the agglomerated state on the photocatalytic hydrogen production with in situ agglomeration of colloidal TiO<sub>2</sub> nanoparticles. *J. Phys. Chem. C* **2008**, *112*, 20451–20457.
- (47) Lim, M.; Chiang, K.; Amal, R. Photochemical synthesis of chlorine gas from iron(III) and chloride solution. *J. Photochem. Photobiol., A* **2006**, *183*, 126–132.
- (48) Nadtochenko, V. A.; Kiwi, J. Photolysis of FeOH<sup>2+</sup> and FeCl<sup>2+</sup> in aqueous solution. Photodissociation kinetics and quantum yields. *Inorg. Chem.* **1998**, *37*, 5233–5238.
- (49) De Laat, J.; Truong Le, G.; Legube, B. A comparative study of the effects of chloride, sulfate and nitrate ions on the rates of decomposition of H<sub>2</sub>O<sub>2</sub> and organic compounds by Fe(II)/H<sub>2</sub>O<sub>2</sub> and Fe(III)/H<sub>2</sub>O<sub>2</sub>. *Chemosphere* **2004**, *55*, 715–723.
- (50) Hsu, C. L.; Wang, S. L.; Tzou, Y. M. Photocatalytic reduction of Cr(VI) in the presence of NO<sub>3</sub><sup>-</sup> and Cl<sup>-</sup> electrolytes as influenced by Fe(III). *Environ. Sci. Technol.* **2007**, *41*, 7907–7914.
- (51) Free, M. L. *Hydrometallurgy: Fundamentals and Applications*; John Wiley & Sons: Hoboken, NJ, 2013.
- (52) Cwiertny, D. M.; Handler, R. M.; Schaefer, M. V.; Grassian, V. H.; Scherer, M. M. Interpreting nanoscale size-effects in aggregated Fe-oxide suspensions: reaction of Fe(II) with goethite. *Geochim. Cosmochim. Acta* **2008**, *72*, 1365–1380.
- (53) Rubasinghege, G.; Kyei, P. K.; Scherer, M. M.; Grassian, V. H. Proton-promoted dissolution of alpha-FeOOH nanorods and micro-rods: Size dependence, anion effects (carbonate and phosphate), aggregation and surface adsorption. *J. Colloid Interface Sci.* **2012**, *385*, 15–23.
- (54) Rubasinghege, G.; Elzey, S.; Baltrusaitis, J.; Jayaweera, P. M.; Grassian, V. H. Reactions on Atmospheric Dust Particles: Surface Photochemistry and Size-Dependent Nanoscale Redox Chemistry. *J. Phys. Chem. Lett.* **2010**, *1*, 1729–1737.